frontiers | Frontiers in Physics

TYPE Original Research
PUBLISHED 23 June 2023
DOI 10.3389/fphy.2023.1195655

OPEN ACCESS

EDITED BY
Yogendra Kumar Prajapati,
Motilal Nehru National Institute of Technology Allahabad, India

REVIEWED BY
Jitendra Bahadur Maurya,
National Institute of Technology Patna, India
Alka Verma,
Institute of Engineering and Rural Technology, Prayagraj (Allahabad), India

*CORRESPONDENCE
Rumao Tao,
supertaozhi@163.com

RECEIVED 28 March 2023
ACCEPTED 06 June 2023
PUBLISHED 23 June 2023

CITATION
Li H, Xie L, Zhang C, Tao R, Shu Q, Li M, Shen B, Feng X, Xu L and Wang J (2023), Metasurface-generating high purity narrow linewidth cylindrical vector beams: power scaling and its limitation. *Front. Phys.* 11:1195655.
doi: 10.3389/fphy.2023.1195655

Metasurface-generating high purity narrow linewidth cylindrical vector beams: power scaling and its limitation

Haokun Li[1,2], Lianghua Xie[2], Chun Zhang[2], Rumao Tao[2]*, Qiang Shu[2], Min Li[2], Benjian Shen[2], Xi Feng[2], Lixin Xu[1] and Jianjun Wang[2]

[1]Department of Optics and Optical Engineering, University of Science and Technology of China, Hefei, China, [2]Laser Fusion Research Center, China Academy of Engineering Physics, Mianyang, China

1.89 kW cylindrical vector beams (CVBs) at 1,064 nm with the 3 dB linewidth being about 0.08 nm have been generated from a narrow linewidth all-fiber linearly-polarized laser by metasurface extra-cavity conversion. At the maximum output power, the transmission efficiency, mode purity of radially polarized cylindrical vector beams (RP-CVBs) are 97% and 92.7%, respectively. To the best of our knowledge, this is the highest power of narrow linewidth CVBs generated from fiber laser. The temperature of the metasurface is moderate, and the maximum temperature is 75.5°C at 1.89 kW, which means that the system can be further power scaled. The evolution of mode purity has been analyzed numerically, and the influence of high-order modes (HOM) in laser source and thermal effects of metasurface has been calculated, which reveals that the presence of high-order modes and the temperature rise of metasurface degrade the mode purity of the CVBs. Among them, HOM causes a degradation of 1.68%, thermal lensing effect contributes 2.32%, and the microstructure variation of the metasurface contributes the remaining 3.3%.

KEYWORDS

cylindrical vector beams, high power, metasurface, fiber laser source, high purity

1 Introduction

Due to the unique polarization and amplitude symmetric properties with highly compact configurations [1, 2], narrow linewidth cylindrical vector beams (CVBs) generated from fiber lasers by intra-cavity or extra-cavity conversion have attracted increasing attention in recent years for its versatile applications, such as material processing [3, 4], optical trapping and manipulation [5–7], high resolution imaging [8, 9], and optical communication [10–12], and so on. Among the aforementioned applications, narrow linewidth CVBs with ever increasing performance figures are demanded, and various methods, including coherent beam combination [13, 14], metasurface [15, 16], grating mirror [17, 18], have been proposed and demonstrated to generate high power CVBs. Among them, it is an efficient and convenient method to generate CVBs by metasurface [19, 20]. In 2014, X. Yi et al presented a simple and efficient method to convert a linearly polarized beam produced by a He–Ne laser to any CVBs based on two cascaded metasurfaces [21]. Then, a 500 W narrow linewidth CVB has already been generated from a linearly polarized fiber laser source by metasurface, which was limited by the output power capability of the employed laser

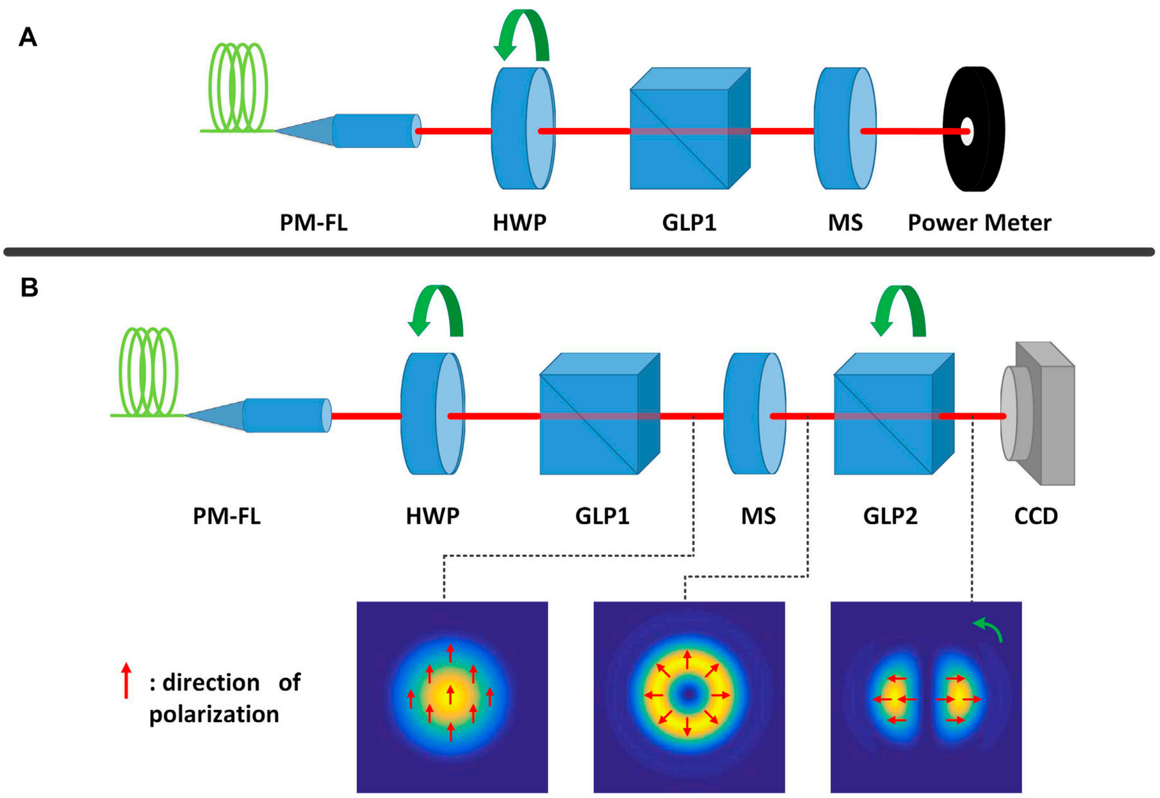

FIGURE 1
Experimental setup to generate and measure CVBs: **(A)** transmission efficiency of metasurface; **(B)** performance of metasurface (PM-FL, polarization maintaining fiber laser; HWP, half-wave plate; GLP, Glan laser prism; MS, metasurface; CCD, charge coupled device.)

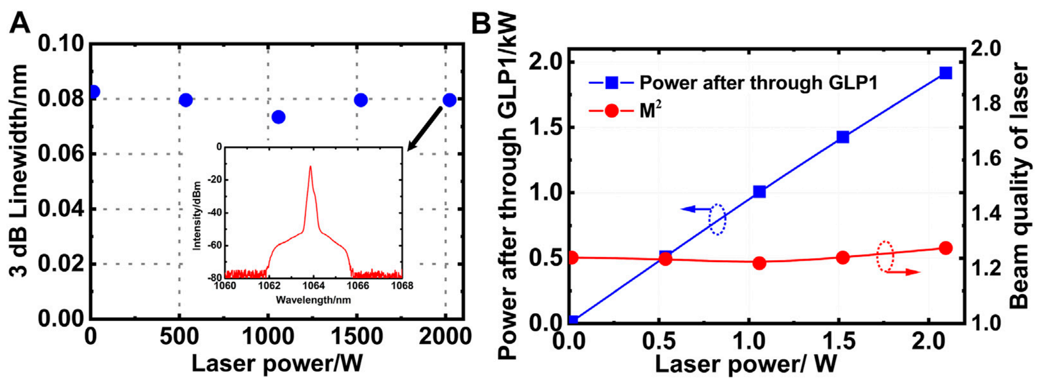

FIGURE 2
Parameters of fiber laser: **(A)** 3 dB linewidth of fiber laser at different output power (inset: spectrum at maximum power); **(B)** M^2 of laser source and power after passing through GLP 1.

sources [15]. Due to that the achieved power level is moderate, the data revealed that no obviously obstacle has been observed, and the possible limitations of generating CVBs with metasurface are still unknown. Fortunately, laser power from narrow linewidth linearly-polarized ytterbium-doped fiber lasers have soared up rapidly in recent years due to the successful mitigating of stimulated Brillouin scattering and transverse mode instability simultaneously [22–25], and 4-kW level narrow linewidth linearly-polarized laser has already been demonstrated [26]. Higher power CVBs can be generated with more powerful linearly-polarized fiber laser sources, which provides the chance to investigate the power scaling capability of the metasurface method and show the road to more powerful CVBs.

In this paper, near 2 kW linearly-polarized narrow linewidth laser was converted into the high-purity radially polarized CVBs

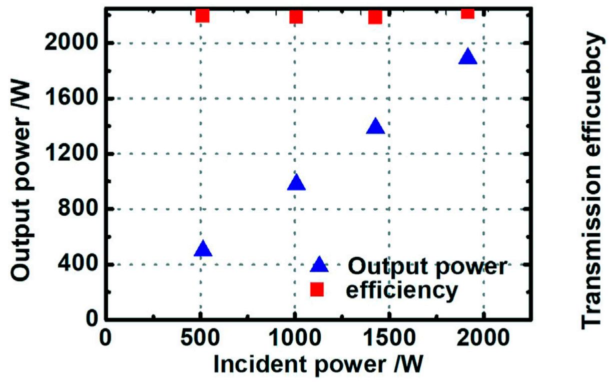

FIGURE 3
The laser power after passing through the metasurface and the transmission efficiency as increasing of incident power.

(RP-CVBs) based on the metasurface with high transmission efficiency. To the best of our knowledge, this is the highest power of CVBs generated from fiber laser. The influence of laser modes on purity of the CVBs has been analyzed, and the power limitation has been discussed.

2 Methods

A metasurface can be regarded as a spatially inhomogeneous phase delay plate with a spatially variable optical axis, and the optical axis of which is set to be parallel to the surface of silica substrate, described with a simplified expression

$$\alpha(r,\varphi) = \frac{1}{2}\varphi \tag{1}$$

where (r, φ) is the polar coordinate representation. The metasurface can lead to a phase retardation δ between the incident electric field with parallel and perpendicular polarization to the optical axis by the effective birefringence effect. Generally, the manipulation of polarization state can be characterized by the multiplication between Jones matrices of an incident beam and metasurface. It should be mentioned that the phase retardation δ is set to be π to realize the conversion from an incident linearly polarized beam to radially polarized beam [21]. Thereby, the Jones matrix T of the metasurface can be written in terms of

$$T(r,\varphi) = \begin{bmatrix} \cos(\varphi) & \sin(\varphi) \\ \sin(\varphi) & -\cos(\varphi) \end{bmatrix} \tag{2}$$

Similarly, the Jones matrix of the linearly polarized Gaussian beam can be expressed by $E_{in}(r,\varphi) = E_0(r,\varphi)\times[\cos(\theta)\ \sin(\theta)]$, where θ is the initial angle between the polarization orientation of the incident linearly polarized beam and the main optical axis direction of the metasurface. After passing through the metasurface, the output beam $E_{out}(r,\varphi) = T(r,\varphi)\,E_{in}(r,\varphi)$ can be deduced by

$$E_{out}(r,\varphi) = E_0(r,\varphi)\begin{bmatrix} \cos(\varphi-\theta) \\ \sin(\varphi-\theta) \end{bmatrix} \tag{3}$$

Therefore, the RP-CVB can be obtained by the linearly polarized beam with the preconditions of $\theta = 0$.

The metasurfaces can have several structures [27], including orthogonal nano-slit pairs arranged [28], rectangle or ellipse silicon resonators [29] and so on. In this paper silicon resonators structure is applied to metasurface. The metasurface is fabricated by writing self-assembled nanostructures in silica glass with a femtosecond laser. The interaction of the plasma with the incident light results in a strip-like nanostructure and the phase retardation is chosen as π. During fabrication, the silica substrate is mounted onto a triaxial translational stage system. This way helps to realize the silicon resonators' optical axis distribution described by Equation 1.

The experimental setup to generate CVBs is shown in Figure 1. To generate narrow linewidth CVBs, a homemade narrow linewidth linear-polarized fiber laser source at 1,064 nm has been employed, which deliverers a maximal laser power of 2095 W with 3 dB linewidth of 0.08 nm. At the maximal output power, the polarization extinction ratio (PER) of the fiber laser is about 10.3 dB, while the beam quality M^2 has been measured to be 1.27 which is not a strictly single mode laser. This is due to that a piece of 1.5 m Germanium doped fiber (GDF) with core diameter being 30 μm has been spliced to deliver the narrow linewidth laser power to avoid the onset of stimulated Brillouin scattering, which

TABLE 1 Comparison of CVBs generated from LP_{01} and LP_{11} laser source.

Laser source	Input-field	Near-field	I_x	I_y	Mode purity (%)
Ideal beam (LP_{01})	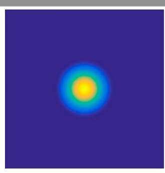	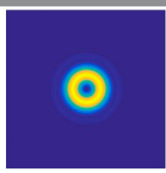	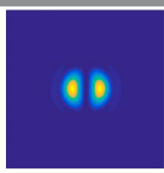	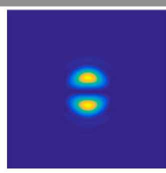	100
High order mode (LP_{11})	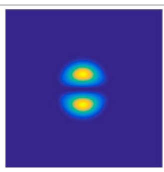	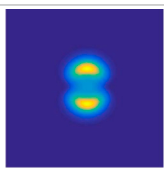	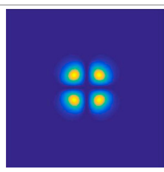	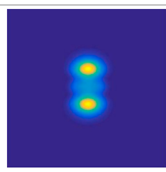	66.65

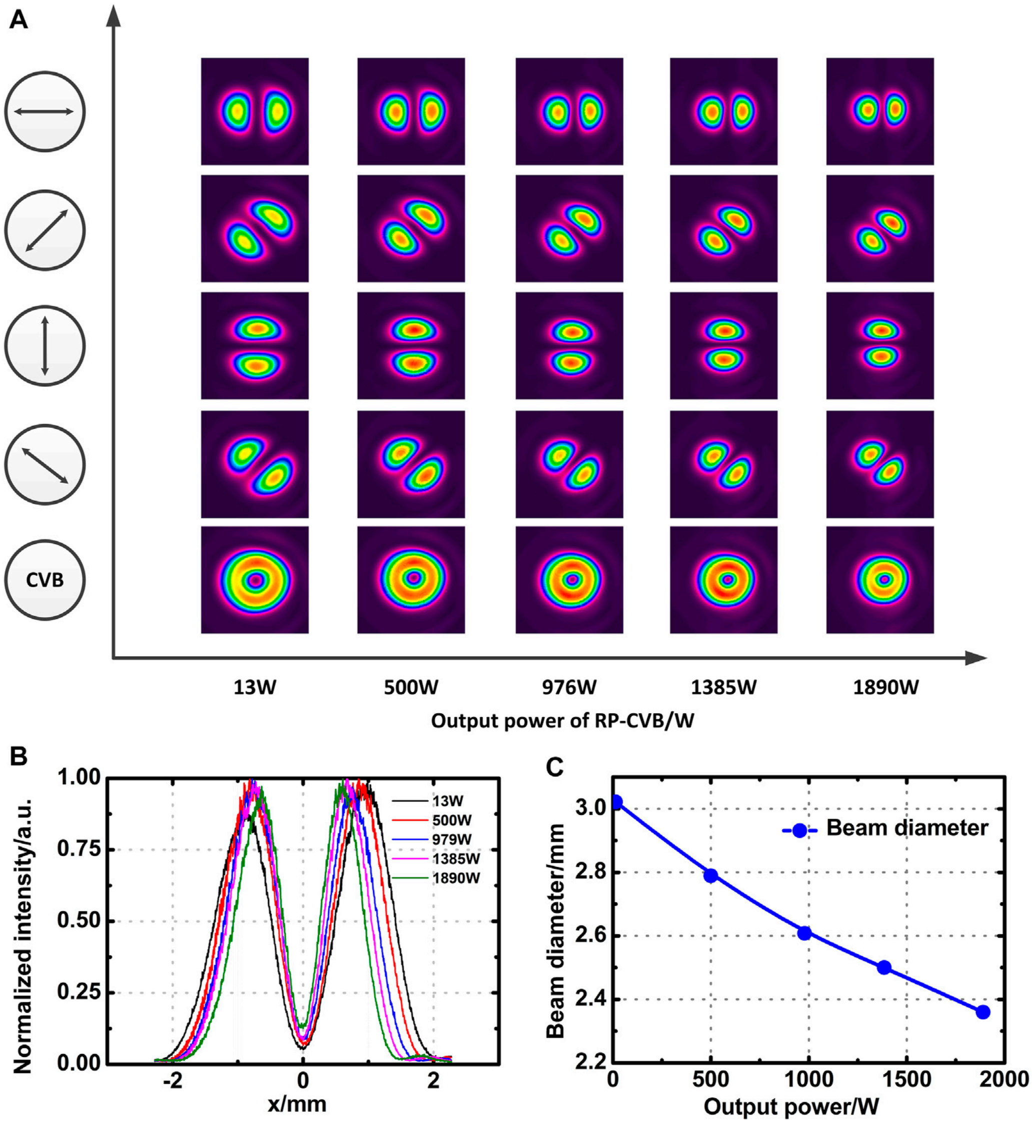

FIGURE 4
(A) Measured laser beam profiles of RP-CVBs generated by metasurface (pictures in 5th line) and after passing through GLP 2 (pictures in 1-4th line) at different output power level (the arrows on the left of vertical axis represent the transmission axis of GLP 2); **(B)** normalized intensity distribution of RP-CVBs along the diameter direction at different output power level; **(C)** beam diameter of RP-CVBs at different output power level.

TABLE 2 The weights and phases of six modal components.

Mode	LP_{01}	LP_{11e}	LP_{11o}	LP_{21e}	LP_{21o}	LP_{02}
Weight	0.851	0.018	0.072	0.007	0	0.052
Phase/rad	0	1.91	1.71	1.39	—	5.97

results to that some amount of power coupling (typically a few percent) from the fundamental LP_{01} mode to higher order modes (HOMs). The excited HOMs have uncontrolled phase and polarization relative to the fundamental mode. Interference of these HOMs with the LP_{01} mode was responsible for the degradation of beam quality that drove up the M^2 values while the depolarization of the HOMs was responsible for the limited PER.

The laser beam has been expanded and collimated with a diameter of 3 mm before projecting onto the metasurface conversion system. A Glan laser prism (GLP 1) was utilized to ensure that the incident beam of the metasurface is completely linear polarized while a rotatable half wave plate (HWP) was employed to adjusting the direction of the injecting laser polarization. Finally, the linear-polarized beam was converted into CVBs by passing through the anti-refection-coated metasurface, which works as a vortex half-wave plate [11], and the aperture diameter of the metasurface is 14 mm. A power meter (PM) was utilized to measure the laser power before and after passing through the metasurface to calculate the transmission efficiency. At last, as shown in Figure 1B, to quantify the performance of metasurface, GLP 2 was placed behind the metasurface to convert the polarization modulation into easily observable intensity modulation. The transmitted intensity

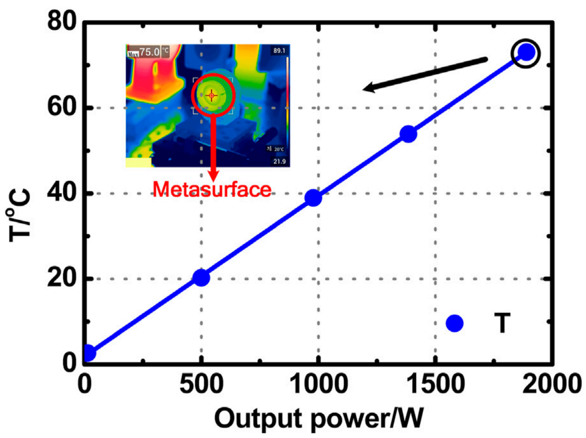

FIGURE 5
Temperature located in the center of metasurface at different output power level (inset: picture caught by infrared thermal imager).

distribution by rotating GLP 2 was recorded by a charge coupled device (CCD).

3 Results

Firstly, the parameters of the linearly-polarized laser were measured, including optical spectrum, beam quality (M^2) and PER. Figure 2A displays the linewidth of the fiber laser at different output power. Figure 2B presents the M^2 of the fiber laser and the laser power after passing through the GLP 1. One can see that the 3 dB linewidth of laser remains about 0.08 nm as the power scaling. M^2 varies from 1.24 to 1.27 as the power increasing, indicating that the laser source has stable and good beam quality. The polarized power after the GLP 1 is 1916 W when the laser source operates at 2095 W, and the measured PER of the laser is 10.3 dB.

The transmission efficiency as increasing of incident power has been shown in Figure 3. One can see that the maximal power of radially polarized beam is 1,890 W, and the maximal average power density is about 27 kW/cm^2 in this experiment. The transmission efficiency of the metasurface is above 98.6%, which shows no sign of degradation or damage, and means that the metasurface can operation stably at multi-kilowatt level with average power density being around 27 kW/cm^2. The transmission loss is induced by several factors, including coating and substrate absorption, light scattering by surface microstructure and so on.

The laser beam profiles of RP-CVBs generated by metasurface and after passing through GLP 2 at different output power level have been recorded. Due to the fact that the intensity distribution of CVBs can almost keep the same over several meters [30], the beam profiles are measured after 1 m free space propagation, which has been plotted in Figure 4. One can conclude that the linearly polarized beams have been converted to RP-CVBs after passing through the metasurface. The profiles of RP-CVBs at different output power level are displayed in the last line of Figure 4A, which manifest as typical "doughnut" intensity distributions. In order to evaluate the quality of RP-CVBs generated in our experiment, the intensity distributions after passing through GLP 2 were measured by CCD, and the measured beam profiles are shown in line 1 to line 4 of Figure 4A. The profiles present the typical shapes of two lobes, which are parallel to the transmitted direction of GLP 2. One can see that the profiles remain the shape of doughnut or two lopes, but gradually shrink as the output power scales. This shrinking is caused by the thermal-lens effect of the metasurface [31]. In order to see more intuitively, the normalized intensity distribution of RP-CVBs along the diameter direction at different output power has been calculated based on the beam profiles of line 5 in Figure 4A, and the results are presented in Figure 4B. The shrinking effect can be observed obviously, and the minimum intensity of central depression area rises with the power scaling, indicating the degradation of CVBs mode purity. Figure 4C shows the beam diameters of RP-CVBs at different output power level, which were calculated with the second-order moment algorithm. One can see that the beam diameters decrease near linearly with the output power increasing.

Furthermore, the surface temperature located in the center of metasurface at different output power level was measured by using an infrared thermal imager. The room temperature was 20°C. As plotted in Figure 5, the maximum temperature reached 75°C at the

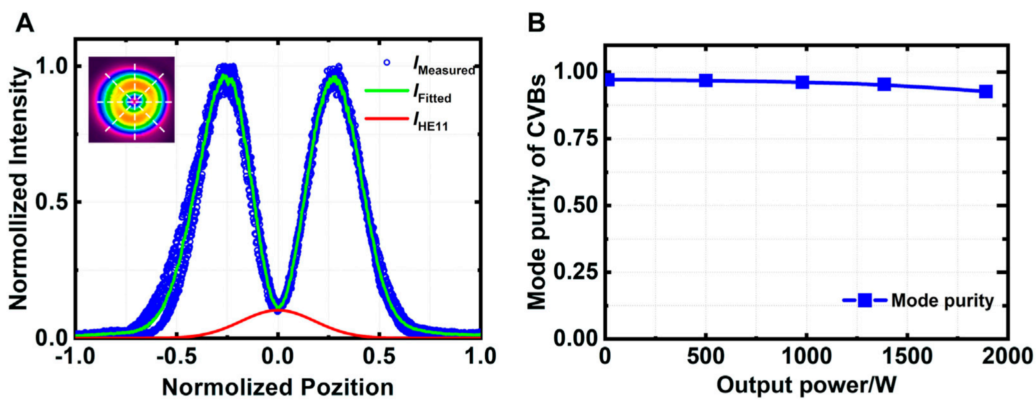

FIGURE 6
(A) Mode purity analysis at output power of 1,890 W (inset: data sampling along the white dashed line); **(B)** mode purity at different output power.

TABLE 3 Comparison of measured beam, reconstructed beam.

	Input-field	Near-field	I_x	I_y	Mode purity (%)
Measured beam	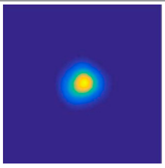	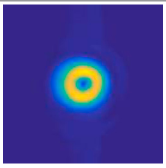	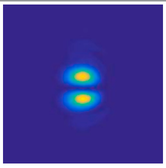	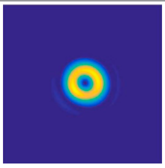	92.70
Reconstructed beam	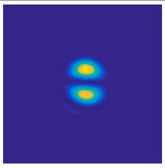	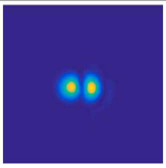	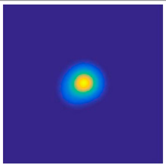	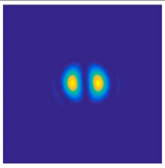	98.32

maximum output power. Considering the linear increment of temperature with the power scaling, it can be fitted with a linear function being $T = 0.0282 \times P_{\mathrm{in}} + 21.43$. The thermal slope is about 28.2°C/kW, agreeing well with the results in Ref. [15].

To evaluate the CVB quantitatively, the one-dimensional intensity distributions of the output beams are fitted by a linear superposition of HE_{11} and TM_{01} modes [32, 33], and the results are shown in Figure 6A. In Figure 6A, the blue circles refer to the measured one-dimensional intensity distribution curve in the radial direction (white lines in inset figure) at the maximal output power while the green line (I_{Fitted}) refers to the average value. The red line (I_{HE11}) refers to the intensity distribution of HE_{11} mode by Gaussian-fitting. It should be mentioned that the peak value of I_{HE11} equals to the value of I_{Fitted} at zero-position. The mode purity of TM_{01} can be obtained by calculating the area enclosed by the above-mentioned two curves [32, 33] in terms of

$$Mode\ Purity = \frac{\int (I_{Fitted} - I_{HE11})dr}{\int I_{Fitted}dr} \tag{4}$$

and the calculated mode purity is 92.7%. The mode purity at different output power level is displayed in Figure 6B, which illustrate that the initial mode purity is about 97.2%. There are several factors leading the deviation of mode purity from 100%, such as the HOMs of the laser source, the defects during processing the metasurface, and so on. As the power scaling, the mode purity decreases from 97.2% to 92.7% which could be attributed by the variation of microstructure with the temperature of metasurface rising [29] and the thermal lens effect.

4 Discussions

To find out the possible physical mechanism of the mode purity gradually degradation as the output power increasing, the impacts of the mode purity of laser source and the thermal-lens effect have been simulated. Due to the fact that the HOMs have stronger gain in fiber laser systems, the power fraction of HOMs increases as laser power increases [34, 35]. The characteristics of CVBs generated from the LP_{01} and LP_{11} laser source has been list in Table 1. The near-field after passing through the metasurface was deduced by the Fresnel diffraction formula.

It can be seen that the mode purity of CVB reaches 100% as the input field be assumed with the ideal beam (LP_{01}), the near field after passing through the metasurface demonstrates a typical "doughnut" intensity distribution. However, as the input field changes to LP_{11} laser source, the central zero strength singularity no longer exists while the mode purity of generated CVB decreases to 66.65%. Thereby, one can conclude that the HOMs power fraction of the laser source can influence the mode purity of CVBs.

Furthermore, in coincide with our experimental results, mode characteristics of the laser source have been analyzed with the mode decomposition technique [36, 37]. Although dozens of modes are supported in the 30/400 μm double-clad fiber, only the first six scalar modes (LP_{01}, LP_{11o}, LP_{11e}, LP_{21o}, LP_{21e}, and LP_{02}) have been taken into consideration, since the power ratio of higher-order modes is negligible. The output beam profile of the fiber laser source under maximum power was measured by the CCD camera at the focal plane, which was employed to deduce the mode characteristics. Based on the stochastic parallel gradient descent (SPGD) algorithm, the mode characteristics are calculated, and the results are listed in Table 2, including the relative weights and phases of six modal components.

Based on the decomposed data in Table 2, the characteristics of CVBs have been deduced, and the simulation results are list in Table 3. It is worth noting that, due to the neglect of higher order modes, the mode decomposition cannot complicatedly restore the measured beam profile of laser sources, which could result in a better mode purity of the CVBs. However, from the first column in Table 3, the restored beam profile is almost the same as the measured one, which proves that the higher order modes of laser source are indeed negligible. The mode purity of CVB generated by the reconstructed light source is 98.32%, meaning that the HOMs of the employed laser source decreases the mode purity of CVBs by 1.68%. Thus, the mode purity of CVB could be further improved by restricting the weight of the HOMs, such as using 20/400 μm GDF to emit laser instead of 30/400 μm GDF.

In the aforementioned discussion, thermal-lens effect of the metasurface has not been taken into consideration, while the metasurface shows obvious temperature rising during power scaling. It is well known that the thermal-lens effect is non-negligible at high-power level, so the influence of thermal-lens effect should be simulated. An equivalent lens was assumed to accommodate the thermal-lens effect of metasurface, and the focal length of which is deduced by fitting the beam diameter data of RP-CVBs at maximal output power. After adding an equivalent lens during the simulation, the mode purity further reduces from 98.32% to 96% at the maximal output power, meaning that the thermal-lens effect in our experiment could result in the decreasing of the mode purity of CVBs by 2.32%. The remain 3.3% degradation of CVBs' mode purity could be induced by the microstructure variation of the metasurface with the temperature rising, the defects during processing the metasurface, ect. Thereby, one can conclude that the power scaling of CVBs is limited by the beam quality of the fiber laser source and the thermal-lens effects of the metasurface. In the future, light source with high beam quality will be employed to improve the quality of CVBs, and cooling devices will be added to metasurface for reducing the thermal effect [38].

5 Conclusion

In summary, we have demonstrated 1890 W RP-CVBs by metasurface extra-cavity conversion in fiber lasers. This is the highest power of narrow linewidth CVBs generated from fiber laser, to the best of our knowledge. The transmission efficiency of metasurface is 97% while the mode purity of generated CVBs is 92.7% at the maximum power, respectively. The temperature of the metasurface has been recorded, which demonstrates the potential for further power scaling. The variation of metasurface's transmission efficiency and the purity of RP-CVBs as power scaling have been measured and calculated, which reveals that the degradation is slight. Furthermore, the physical origin of the purity degradation has been investigated, and the simulation results indicate that the HOMs in laser source and the temperature rise of the metasurface can degrade the mode purity of the CVBs. Among them, HOM causes a degradation of 1.68%, thermal lensing effect contributes 2.32%, and the microstructure variation of the metasurface contributes the remaining 3.3%. Thereby, the further power scaling of the CVBs generated by metasurface extra-cavity conversion in fiber lasers are mainly limited by the power scalability of single mode linearly-polarized laser source and the thermal-lens effect in free-space optics. In general, a stable and flexible approach is presented to generate high-power CVBs, and we believe that it can promote the applications of CVBs, such as material processing, science research, etc.

Data availability statement

The original contributions presented in the study are included in the article/supplementary material, further inquiries can be directed to the corresponding author.

Author contributions

HL and RT contributed to conception and design of the study. HL organized the database. HL, LX and CZ performed the statistical analysis. HL wrote the first draft of the manuscript. RT wrote sections of the manuscript. All authors contributed to the article and approved the submitted version.

Funding

This work was supported by the National Natural Science Foundation of China (NSFC) (61905226), and the Youth Talent Climbing Foundation of the Laser Fusion Research Center.

Conflict of interest

The authors declare that the research was conducted in the absence of any commercial or financial relationships that could be construed as a potential conflict of interest.

Publisher's note

References

1. Zhan QW. Cylindrical vector beams: From mathematical concepts to applications. *Adv Opt Photon* (2009) 1(1):1–57. doi:10.1364/aop.1.000001

2. Chen SZ, Zhou XX, Liu YC, Ling XH, Luo HL, Wen SC. Generation of arbitrary cylindrical vector beams on the higher order poincare sphere. *Opt Lett* (2014) 39(18): 5274–6. doi:10.1364/ol.39.005274

3. Kozawa Y, Sato M, Uesugi Y, Sato S. Laser microprocessing of metal surfaces using a tightly focused radially polarized beam. *Opt Lett* (2020) 45(22):6234–7. doi:10.1364/ol.405852

4. Meier M, Romano V, Feurer T. Material processing with pulsed radially and azimuthally polarized laser radiation. *Appl Phys A* (2007) 86(3):329–34. doi:10.1007/s00339-006-3784-9

5. Otte E, Denz C. Optical trapping gets structure: Structured light for advanced optical manipulation. *Appl Phys Rev* (2020) 7(4):041308. doi:10.1063/5.0013276

6. Zhan QW. Trapping metallic Rayleigh particles with radial polarization. *Opt Express* (2004) 12(15):3377–82. doi:10.1364/opex.12.003377

7. Zhang YR, Chang CL, Yuan CJ, Feng ST, Nie SP, Ding JP. Composite generation of independently controllable multiple three-dimensional vector focal curve beams. *OPTICS COMMUNICATIONS* (2019) 450:296–303. doi:10.1016/j.optcom.2019.06.021

8. Kozawa Y, Sato S. Numerical analysis of resolution enhancement in laser scanning microscopy using a radially polarized beam. *Opt Express* (2015) 23(3):2076–84. doi:10.1364/oe.23.002076

9. Segawa S, Kozawa Y, Sato S. Resolution enhancement of confocal microscopy by subtraction method with vector beams. *Opt Lett* (2014) 39(11):3118–21. doi:10.1364/ol.39.003118

10. Milione G, Mpj L, Huang H, Ren YX, Xie GD, Nguyen TA, et al. 4 × 20 Gbit/s mode division multiplexing over free space using vector modes and a q-plate mode (de) multiplexer. *Opt Lett* (2015) 40(9):1980–3. doi:10.1364/ol.40.001980

11. Wang CF, Yang B, Cheng ML, Cheng SH, Liu JM, Xiao JN, et al. Cylindrical vector beam multiplexing for radio-over-fiber communication with dielectric metasurfaces. *Opt Express* (2020) 28(26):38666–81. doi:10.1364/oe.406300

12. Yue ZY, Lu PY, Xu JL, Li Z, Teng SY. Vector beams encoded by diverse orthogonal polarization states and their generation based on metasurfaces. *NEW JOURNAL PHYSICS* (2023) 25(1):013018. doi:10.1088/1367-2630/aca787

13. Ma PF, Zhou P, Ma YX, Wang XL, Su RT, Liu ZJ. Generation of azimuthally and radially polarized beams by coherent polarization beam combination. *Opt Lett* (2012) 37(13):2658–60. doi:10.1364/ol.37.002658

14. Zhang YQ, Hou TY, Chang HX, Yu T, Chang Q, Jiang M, et al. Tight focusing properties and focal field tailoring of cylindrical vector beams generated from a linearly polarized coherent beam array. *Opt Express* (2021) 29(4):5259–69. doi:10.1364/oe.417038

15. Xie LH, Tao RM, Guo C, Chu QH, Zhang C, Li HK, et al. High-power cylindrical vector beams generated from an all-fiber linearly polarized laser by metasurface extracavity conversion. *Appl Opt* (2021) 60(24):7346–61. doi:10.1364/ao.431393

16. Liu D, Zhou C, Lu P, Xu J, Yue Z, Teng S. Generation of vector beams with different polarization singularities based on metasurfaces. *New J Phys* (2022) 24(4): 043022. doi:10.1088/1367-2630/ac60dd

17. Ahmed MA, Schulz J, Voss A, Parriaux O, Pommier JC, Graf T. Radially polarized 3kW beam from a CO_2 laser with an intracavity resonant grating mirror. *Opt Lett* (2007) 32(13):1824–6. doi:10.1364/ol.32.001824

18. Dietrich T, Rumpel M, Beirow F, Mateo CM, Pruss C, Osten W, et al. Thin-disk oscillator delivering radially polarized beams with up to 980 W of cw output power. *Opt Lett* (2018) 43(6):1371–4. doi:10.1364/ol.43.001371

19. Wang JJ, Pu MB, Jin JJ, Zhang F, Liu L, Kong WJ, et al. Generation of a space-variant vector beam with catenary-shaped polarization states. *Materials* (2022) 15(8): 2940. doi:10.3390/ma15082940

20. Yan J, Guo YH, Pu MB, Li X, Ma XL, Luo XG. High-efficiency multi-wavelength metasurface with complete independent phase control. *Chin Opt Lett* (2018) 16(5): 050003. doi:10.3788/col201816.050003

21. Yi XN, Ling XH, Zhang ZY, Li Y, Zhou XX, Liu YC, et al. Generation of cylindrical vector vortex beams by two cascaded metasurfaces. *OPTICS EXPRESS* (2014) 22(14): 17207–15. doi:10.1364/OE.22.017207

22. Tao RM, Ma PF, Wang XL, Zhou P, Liu ZJ. 1.3 Kw monolithic linearly polarized single-mode master oscillator power amplifier and strategies for mitigating mode instabilities. *Photon Res* (2015) 3(3):86–93. doi:10.1364/prj.3.000086

23. Ma PF, Tao RM, Su RT, Wang XL, Zhou P, Liu ZJ. 1.89 Kw all-fiberized and polarization-maintained amplifiers with narrow linewidth and near-diffraction-limited beam quality. *Opt Express* (2016) 24(4):4187–95. doi:10.1364/oe.24.004187

24. Su RT, Tao RM, Wang XL, Zhang HW, Ma PF, Zhou P, et al. 2.43 Kw narrow linewidth linearly polarized all-fiber amplifier based on mode instability suppression. *Laser Phys Lett* (2017) 14(8):085102. doi:10.1088/1612-202X/aa760b

25. Wang YS, Sun YH, Peng WJ, Feng YJ, Wang J, Ma Y, et al. 3.25 Kw all-fiberized and polarization-maintained Yb-doped amplifier with a 20 Ghz linewidth and near-diffraction-limited beam quality. *Appl Opt* (2021) 60(21):6331–6. doi:10.1364/ao.431081

26. Ren S, Ma PF, Li W, Wang GJ, Chen YS, Song JX, et al. 3.96 Kw all-fiberized linearly polarized and narrow linewidth fiber laser with near-diffraction-limited beam quality. *Nanomaterials* (2022) 12(15):2541. doi:10.3390/nano12152541

27. Wang J, Du J. Plasmonic and dielectric metasurfaces: Design, fabrication and applications. *APPLIED SCIENCES-BASEL* (2016) 6(9):239. doi:10.3390/app6090239

28. Zeng XY, Zhang YQ, Zhang RR, Ren XR, Zhan ZJ, Gu MN, et al. Generation of vector beams of bell-like states by manipulating vector vortex modes with plasmonic metasurfaces. *OPTICS LETTERS* (2021) 46(3):528–31. doi:10.1364/OL.415981

29. Arbabi A, Horie Y, Bagheri M, Faraon A. Dielectric metasurfaces for complete control of phase and polarization with subwavelength spatial resolution and high transmission. *NATURE NANOTECHNOLOGY* (2015) 10(11):937–43. doi:10.1038/NNANO.2015.186

30. Liu XZ, Zhang YM, Dong ZP, Lv JL, Dai CS, Luo J, et al. High-power cylindrical vector beam fiber laser based on an all-polarization-maintaining structure. *Opt Express* (2022) 30(15):27123–31. doi:10.1364/oe.463667

31. CS Zhang, ZL Shi, B Feng, BS Xu, editors. *Infrared lens thermal effect: Equivalent focal shift and calculating model. International symposium on optoelectronic Technology and application (IPTA) - infrared Technology and applications*; 2014 May 13-15; Beijing, PEOPLES R CHINA: Proc. SPIE (2014).

32. Li L, Wang M, Liu T, Leng JY, Zhou P, Chen JB. High-power, cladding-pumped all-fiber laser with selective transverse mode generation property. *Appl Opt* (2017) 56(17):4967–70. doi:10.1364/ao.56.004967

33. Zhang YM, Tao RX, Li HX, Fang WT, Dong ZP, Dai CS, et al. Stable generation of cylindrical vector beams with an all-fiber laser using polarization-maintaining and ring-core fibers. *Opt Express* (2020) 28(12):18351–9. doi:10.1364/oe.395757

34. Gong ML, Yuan YY, Li C, Yan P, Zhang HT, Liao SY. Numerical modeling of transverse mode competition in strongly pumped multimode fiber lasers and amplifiers. *Opt Express* (2007) 15(6):3236–46. doi:10.1364/oe.15.003236

35. Tao RM, Liu Y, Xie LH, Gao C, Li M, Shen BJ, et al. Static and dynamic mode evolution in high-power distributed side-coupled cladding-pumped fiber amplifiers. *High Power Laser Sci Eng* (2021) 9:e58. doi:10.1017/hpl.2021.44

36. Huang LJ, Guo SF, Leng JY, Lu HB, Zhou P, Cheng X. Real-time mode decomposition for few-mode fiber based on numerical method. *Opt Express* (2015) 23(4):4620–9. doi:10.1364/oe.23.004620

37. Zhang C, Chu QH, Feng X, Xie LH, Liu Y, Li HK, et al. Mode evolution of high power monolithic Pm fiber amplifiers in the presence of srs effect. *Ieee Photon Technol Lett* (2022) 34(4):215–8. doi:10.1109/lpt.2022.3148999

38. Muller M, Aleshire C, Klenke A, Haddad E, Legare F, Tunnermann A, et al. 10.4 Kw coherently combined ultrafast fiber laser. *Opt Lett* (2020) 45(11):3083–6. doi:10.1364/ol.392843